ChemComm

Accepted Manuscript

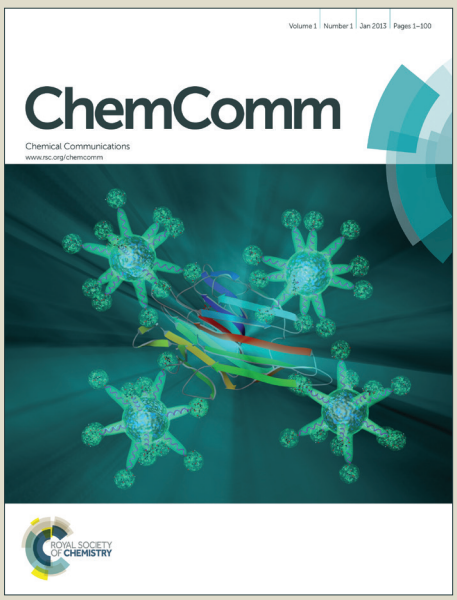

ROYAL SOCIETY OF CHEMISTRY

www.rsc.org/chemcomm

Journal Name

RSCPublishing

COMMUNICATION

Cheap Carbon Black-based High-performance Electrocatalysts for Oxygen Reduction Reaction

Cite this: DOI: 10.1039/xoxxoooooox

Received ooth January 2012,
Accepted ooth January 2012

DOI: 10.1039/xoxxoooooox

www.rsc.org/

Ping Song,[a] Yuwei Zhang,[a] Jing Pan,[b] Lin Zhuang[b] and Weilin Xu[a,*]

A family of cheap carbon black based Fe-N_x/C electrocatalysts with superhigh-performance for oxygen reduction reaction (ORR) were synthesized. The one with Fe 10 wt. % and N 1.57 wt. % shows the best performance. The activity order of different active sites for ORR was revealed firstly: Fe-$N_{4/2}$-C > Fe_4-N-C > N-C >> Fe_4-C ≈ C.

For the commercialization of fuel cell industry, one of the main obstacles is the ORR on cathode due to its sluggish kinetic process on platinum (Pt).[1-3] The scarcity of Pt and its poor stability and tolerance to carbon monoxide (CO) or other organic molecules in cathode have severely hindered the commercialization of the fuel cells.[4, 5] It has been found that the addition of certain cheap metals (e.g., Fe, Co, Mn and Zn) to nitrogen-doped carbon frameworks can result in an efficient nonprecious metal catalyst system for ORR in alkaline or acidic media[3, 6-143, 6-143, 6-143, 6-143, 6-143, 6-143, 6-143, 6-14] However, most of them are still expensive in cost due to the rarity of the carbon materials used or the complexity of the synthesis process.[3, 10] It has been known the ORR activity of these non-precious metal catalysts is strongly dependent on the choice of precursors for carbon, nitrogen and transition-metals, and the exact synthesis procedures utilized.[15, 16] Here by varying the pretreatment of carbon black, a new kind of optimized Fe-N_x/C catalyst with higher ORR performance on alkaline fuel cells was obtained with cheap carbon black, urea and $FeCl_3$ $6H_2O$. Due to the higher performance and lower cost compared with previous best Fe-N_x/C,[9] the obtained ORR catalyst here possesses one of the best performance/price ratios ever and then is one of the most promising alternatives to Pt for ADMFC.

For the synthesis of Fe-N_x/C, the cheap Black Pearls 2000 (BP) was oxidized first with HNO_3 to induce more oxygen species on carbon (Supporting Information (SI), Fig. S1). The oxidized BP (BP_{ox}) was used as support; cheap urea and $FeCl_3$ were used as N and Fe precursors, respectively, to dope BP_{ox} at 900°C under the argon flow.[9] For comparison, BP_{ox}-N was also obtained in a similar way (SI).

The ORR activities for these catalysts have been evaluated by cyclic voltammetry (CV) and linear sweep voltammetry (LSV) on a rotating ring disk electrode (RRDE) in 0.1 M KOH solution. The onset potential (E_{onset}) or half-wave potential ($E_{1/2}$) from LSV has been extracted for each catalyst for comparison. As shown in Fig. S2, the oxidation pretreatment can greatly improve the ORR activity of carbon indicated by the 80mV positive shift of E_{onset} although it is still a two-step two-electron ORR process. The reason for the improvement probably could be attributed to the oxygen species induced on carbon surface and the removal of some unstable amorphous carbon.[6] Since the oxidation can improve the activity of carbon support, then the BP_{ox} was used as support in the following experiments.

Firstly, the optimal carbon/urea mass ratio (C/U) was found to be about 1:10 as shown in Fig. 1a at two different Fe contents. Based on this optimal C/U ratio of 1:10 with final N content of 1.57 wt. % (Fig. S3), we varied the Fe content from 0.02 wt. % to 15 wt. %. As shown in Figure 1b, the data show the Fe-content dependence of the catalytic activity of these catalysts with three local maximums at Fe 1 wt. %, 3 wt. %, and 10 wt. %, respectively, in which the global maximum is at Fe 10 wt. % with E_{onset} at 1.07 V vs. RHE.

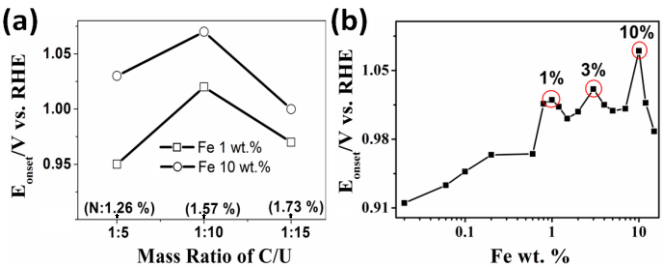

Fig. 1. The optimization of BP_{ox}-NFe catalysts. (a) The initial mass ratio between carbon and urea (C/U) dependence of the catalyst performance at different fixed Fe contents. The corresponding N content (wt. %) was also noted on it. (b) Fe-content dependence of BP_{ox}-NFe catalysts with C/U ratio of 1:10. The three red circles indicate three local maximums.

As an example, the global optimal BP_{ox}-NFe with C/U ratio of 1:10 and Fe 10 wt.% was introduced in detail as following. As shown in Fig. 2a-d, the pure BP_{ox} in 0.1 M KOH is sluggish for ORR with low onset potential at about 0.84 V vs. RHE and a two-step two-electron process with high yield (60%) of H_2O_2. As expected, the pure N-doping on BP_{ox} can promote the ORR process indicated by a higher onset potential at about 0.90 V and a four-electron ORR process with much lower H_2O_2 yield. Furthermore, for the co-doping of BP_{ox} with both N and Fe, as expectedly, the ORR activity on

BP_{ox}-NFe was greatly enhanced due to a well-known synergetic effect between doped N and Fe.[17] CV shows a peak potential at 0.87 V, which is 70mV higher than that (0.80 V) on commercial Pt/C or other best non-Pt ORR catalysts,[2] suggesting a pronounced electrocatalytic activity of BP_{ox}-NFe for ORR. Interestingly, a small ORR peak current on BP_{ox}-NFe was obtained compared with BP_{ox}-N. The reason probably could be attributed to the small Brunauer–Emmett–Teller (BET) surface area (1100 m^2/g) of BP_{ox}-NFe compared with that (1600 m^2/g) of BP_{ox}-N. From LSV, the higher onset potential (1.07 V) than that (0.96 V) on Pt/C further confirms the high performance of BP_{ox}-NFe for ORR in alkaline condition. The limiting ORR current on Pt/C declines slight at potentials lower than 0.6 V, which probably could be attributed to the deactivated Pt nanoparticles or other active sites take part in the ORR as two-electron (2e) catalytic process leading to the production of more H_2O_2, which prevents the direct 4e production of diffused oxygen molecules at Pt nanocatalyst.[18] Typical LSV curves on RRDE at different rotation rates are shown in Fig. 2e. The limiting-current shows a typical increase with rotation rate due to the shortened diffusion layer.[19] Analysis (SI) of the currents obtained from both disk electrode and ring electrode reveals a four-electron process (n≈3.9) of the ORR on BP_{ox}-NFe, with very low H_2O_2 yield and water as the main product, as is the case for Pt-based catalysts. To the best of our knowledge, the optimal BP_{ox}-NFe presented here is one of the best ORR catalysts in alkaline to date (Table S1).[6]

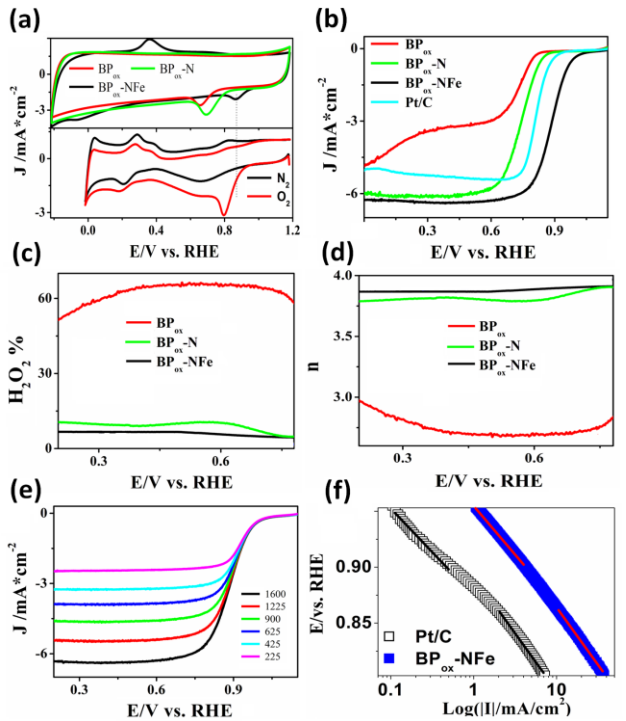

Fig. 2. Electrochemical characterization of BP_{ox}-NFe. (a) Up: CVs of pure BP_{ox}, BP_{ox}-N, and BP_{ox}-NFe in O_2-saturated 0.1 M KOH with scan rate of 50 mV/s; bottom: CVs of Pt/C with or without O_2. (b) RRDE polarization curves of pure BP_{ox}, BP_{ox}-N, and BP_{ox}-NFe and Pt/C in O_2-saturated 0.1 M KOH with scan rate of 5 mV/s and rotation speed of 1600 rpm. (c), (d) The H_2O_2 yield and the electron transfer number (n) on different catalysts of pure BP_{ox}, BP_{ox}-N, and BP_{ox}-NFe. (e) LSV for oxygen reduction on BP_{ox}-NFe in O_2-saturated 0.1 M KOH at various rotation speeds with scan rate of 5 mV/s. (f) Diffusion-corrected Tafel plots for BP_{ox}-NFe and Pt/C extracted from (b); the current "I" equals $i_L i/(i-i_L)$, i_L is the limiting current. The loadings of catalysts are 0.39 mg cm^{-2} for doped carbon catalysts and 24 ug $_{Pt}$ cm^{-2} for commercial Pt/C.

The performance of optimal BP_{ox}-NFe was further evaluated for mechanistic and kinetic performance using diffusion-corrected Tafel plots (Fig. 2f). The Tafel slop in the low current density region on BP_{ox}-NFe is 70 mV/decade, which is close to that (67 mV/decade) on Pt/C surface. This reveals the transfer of the first electron on both of these two catalysts is the rate-determining step under Temkin conditions for the adsorption of intermediates.[9] In the high current density region, the Tafel slop is 94 mV/decade, which is slightly smaller than that (96 mV/decade) on Pt/C surface. This result is attributed to a change in the mechanism of ORR from Temkin to Langmuir adsorption conditions when the current density increases.[20] From a mechanistic point of view, this would imply the ORR mechanisms on BP_{ox}-NFe and Pt-based catalysts are similar in an alkaline medium.[21] In addition, the smaller Tafel slop of BP_{ox}-NFe than Pt/C at high current density reveals that overpotential increases slowly with current density, leading to better ORR activity of BP_{ox}-NFe.[22] A 96-times higher exchange current density (9.6×10^{-3} mA/cm^2) of BP_{ox}-NFe was obtained from Tafel plots when compared with the exchange current density (1.0×10^{-4} mA/cm^2) of commercial 20 wt % Pt/C, indicating a higher intrinsic activity of BP_{ox}-NFe for the ORR than commercial Pt/C.

Based on the US Department of Energy's accelerated durability test protocol, we assessed the durability or stability of the BP_{ox}-NFe catalyst by cycling the catalyst between 0.6 and 1.0 V at 200 mV s^{-1} in an O_2 saturated 0.1 M KOH.[6, 14] As shown in Fig. 3a, a 15 mV negative shift of $E_{1/2}$ after 30,000 cycles (curve *A*→*B*) shows the deterioration of BP_{ox}-NFe due to the collapsing of some N- or Fe-based active sites, much small than the 32 mV negative shift on Pt/C after only 6,000 cycles,[9, 23, 24] thus exhibiting excellent long-term operation stability.

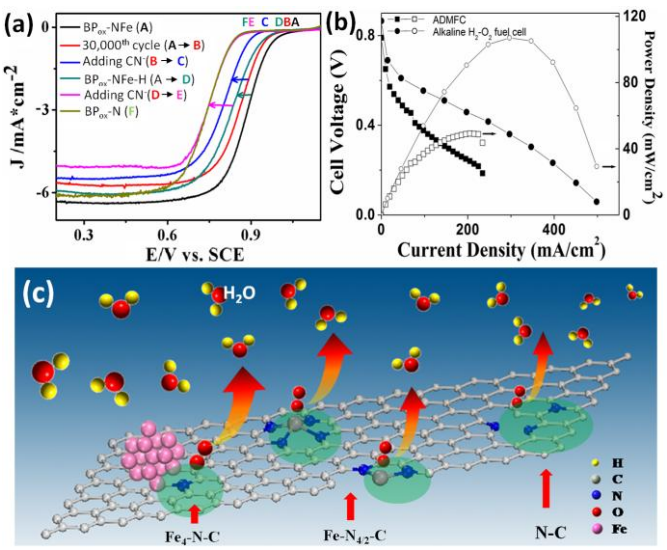

Fig. 3. (a) RDE polarization curves of different catalysts with scan rate of 5 mV/s in O_2-saturated 0.1 M KOH. Letters of *A*, *B*, *C*, *D*, *E*, and *F* in different colours indicate different catalysts. (b)The performance of ADMFC (60°C, square) and alkaline H_2-O_2 (50°C, circle) fuel cell with optimal BP_{ox}-NFe as cathodes. Anode: Pt/C. (c) The scheme to show three main active sites related to doped N on Fe-N_x/C catalysts for ORR.

In order to further substantiate the high performance of BP_{ox}-NFe observed above in alkaline solution; we performed alkaline direct methanol fuel cell (ADMFC) and alkaline H_2-O_2 fuel cell tests with BP_{ox}-NFe as cathodes, respectively (SI). As shown in Fig. 3b, the ADMFC with BP_{ox}-NFe as cathode catalyst shows a high performance with open circuit voltage of 0.80 V and maximum power density (P_{max}) of ~49.2 mW/cm^2 at 60°C,[25] which are the best values among all the non-Pt ORR catalysts on ADMFC reported ever (Fig. S4).[9, 23, 24] The high ORR performance of the optimal BP_{ox}-NFe was further confirmed on alkaline H_2-O_2 fuel cell (Table

S2). As shown in Fig. 3b, the P_{max} with optimal BP_{ox}-NFe as cathode could be up to 107 mW/cm^2 at 50°C with no backpressure. All these data further substantiate the high performance of BP_{ox}-NFe as an ORR catalyst in alkaline medium, and unambiguously indicate the BP_{ox}-NFe is an excellent alternative to Pt as a cathode catalyst in alkaline fuel cells, whether it be a performance or cost point of view.

Furthermore, the optimal BP_{ox}-NFe was found to be highly active for ORR in acidic condition as well. As shown in Fig. S5, in 0.5 M H_2SO_4, the onset potential for the four-electron ORR process on BP_{ox}-NFe is approximately 0.89 V vs. RHE, which is on the same level as other reported best non-Pt-based ORR catalysts in acid [14] and only 70mV lower than commercial Pt/C. Up to now, there are many reports about Fe-N_x/C electrocatalysts for ORR, but very few of them are highly active in both alkaline and acidic conditions.[3, 9]

In order to assess the role of iron in forming active ORR catalytic sites on BP_{ox}-NFe catalysts, we investigated the ORR activity of BP_{ox}-NFe in 0.1 M KOH containing 10 mM KCN after 30,000 cycles (Fig. 3a). CN^- ions are known to coordinate strongly with Fe and poison the Fe-centred (Fe-$N_{4/2}$-C) catalytic sites for ORR.[17] With the addition of CN^-, the ORR half-wave potential of BP_{ox}-NFe catalyst decreases significantly by 64 mV (*B*→*C*), with a little decrease in the diffusion-limiting current, suggesting blocking of part of the Fe-centered active sites by CN^- ions. Interestingly, the residual activity of CN^--poisoned BP_{ox}-NFe is still on the same level as Pt/C (Fig. S6).

Since all the atomically-dispersed Fe-centered active sites (Fe-$N_{4/2}$-C, standing for FeN_2-C or FeN_4-C as shown in Fig. 3c) have been poisoned by CN^- and the pure N-doping on BP_{ox} only can induce very limited ORR activity as shown in Fig. 3a, the high residual activity of CN^--poisoned BP_{ox}-NFe (blue curve *C* in Fig. 3a) probably could be mainly attributed to some special Fe atoms on Fe nanoparticle surface with special microenvironment. First, these special surface Fe atoms strongly bond with other Fe atoms inside the nanoparticle. The bonding makes these surface Fe atoms inert to CN^- complexing action due to the steric hindrance. Secondly, these surface "inert" Fe atoms need to be very close to some N atoms doped on carbon (N-C) to form a new type of active site noted as Fe_4-N-C (Fe_4 stands for both Fe^0 and iron oxide nanoparticles) shown in Fig. 3c.[10] The pure carbon surface attached by Fe nanoparticles (Fe_4-C) is almost inert to ORR as carbon (C) shown before.[9] Actually the model presented here coincides with previous theoretical prediction that the doped N on carbon can tremendously activate the nearby carbon-supported Fe nanoparticles for ORR.[10] That means, in the N, Fe-co-doped catalysts, besides the well-known active sites from N-C, Fe-$N_{4/2}$-C,[26] the Fe_4-N-C is the third type of active site possessing high intrinsic activity, evident by the high residual ORR activity of poisoned BP_{ox}-NFe (blue curve *C*) shown on LSV in Fig. 3a. Based on this fact it can be inferred that three types of active sites always co-exist in Fe-N_x/C catalysts related to N (Fig. 3c). When Fe content is high, the Fe_4-N-C active sites may dominate the whole activity of catalysts. While at extremely low Fe content, just like that shown before, the active sites of N-C and Fe-$N_{4/2}$-C dominate the whole ORR activity.[9]

In order to quantify the contribution of iron nanoparticle (Fe_4-N-C/Fe_4-C) to the ORR process, HCl was used to treat fresh BP_{ox}-NFe since it has been known that the HCl treatment can destroy Fe_4-N-C/Fe_4-C active sites by dissolving iron (Fe^0 and iron oxide) nanoparticles (Fe_4).[3] As shown in Fig. 3a, after the HCl treatment, the half-wave potential on BP_{ox}-NFe-H negatively shifted 50 mV (*A*→*D*), which is smaller than that (64 mV) of KCN-induced poisoning (*B*→*C*), indicating that the intrinsic activity of Fe-$N_{4/2}$-C active sites is higher than that of Fe_4-N-C/Fe_4-C. After HCl treatment, the dominant active sites on BP_{ox}-NFe-H are Fe-$N_{4/2}$-C and N-C sites. Then, KCN was added to further poison the Fe-$N_{4/2}$-C sites on BP_{ox}-NFe-H and only N-C active sites were left (*E*). Interestingly, after the poisoning, the half-wave potential of BP_{ox}-NFe-H negatively shifted 68 mV (*D*→*E*), which is close to the negative shift of 64 mV observed above from curve *B*→*C* with KCN poisoning and could be firmly attributed to the loss of Fe-$N_{4/2}$-C active sites. Moreover, after the removing of Fe_4-N-C/Fe_4-C sites with HCl treatment and Fe-$N_{4/2}$-C sites with KCN, the only left N-C sites (*E*) show similar activity to that on BP_{ox}-N which only possesses N-C active sites (*F*). In addition, the residual activity of CN^--poisoned BP_{ox}-NFe (*C*) is much higher than that of BP_{ox}-N with only N-C sites (*F*), indicating the Fe_4-N-C active sites possess higher intrinsic ORR activity compared with N-C sites.[10] Based on all these facts, the following catalytic activity order for different active sites could be deduced: Fe-$N_{4/2}$-C > Fe_4-N-C > N-C >> Fe_4-C ≈ C.

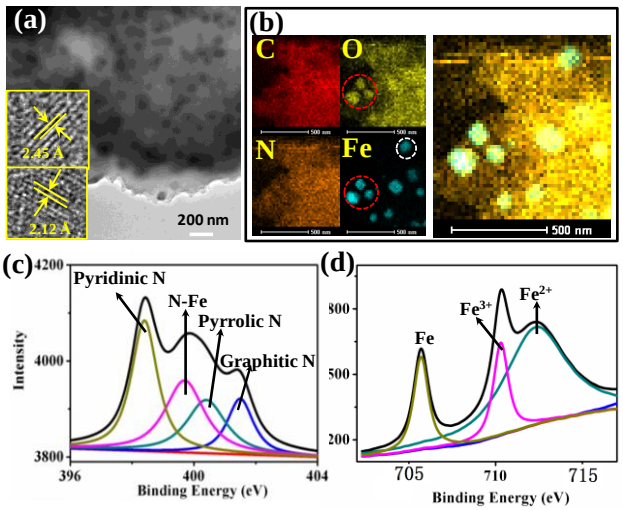

Fig. 4. The physical characterization of BP_{ox}-NFe. (a)(b) TEM images and EDX mapping to show the existence of Fe oxide and Fe^0 nanoparticles on carbon support. (c)(d) The high resolution XPS spectra of N 1s and Fe2p.

To get more insight into the higher electrocatalytic activity of BP_{ox}-NFe, some detailed physical characterizations have been done as following. The Raman Spectra (Fig. S7) show the co-doping of N, Fe did not change much the morphology of carbon support. As shown in Fig. 4a,b, the transmission electron microscopy (TEM) images clearly show the Fe nanoparticles formed on amorphous carbon support. The high-resolution transmission electron microscopy (HRTEM) images reveals the diffraction fringe of Fe nanoparticles (Insert in Fig. 4a), and the measured interplanar spacings are about 0.25 nm and 0.21 nm, which could be assigned to Fe_3O_4 (311) and Fe^0 (111), respectively. As for the EDX mapping shown in Fig. 4b, it can be seen the O and N elements are evenly distributed on carbon support, while the Fe mainly exists in the form of nanoparticle aggregations. Interestingly, from O and Fe mappings, we can see some Fe nanoparticles are iron oxides such as Fe_3O_4 indicated by the red circles, while some others are mainly in Fe^0 state (white circle) since there is no obvious oxygen aggregation in the area corresponding to these nanoparticles on oxygen mapping. This is consistent with HRTEM images shown in Fig. 4a and the X-ray photoelectron spectroscopy (XPS) results shown in the following Fig. 4d. Due to the limited resolution of this TEM microscopy, atomically-dispersed Fe atoms or active sites on Fe mapping could not be discriminated. From C mapping, no shade can be seen in the area of Fe nanoparticles, indicating these Fe nanoparticles were covered by a thin layer of carbon film.[27] The protection of these carbon covers against the oxidation of Fe nanoparticles could explain the superstability of the catalyst shown in Fig. 3a.[10] On the other hand, the N is evenly distributed among the whole area

including the Fe nanoparticle surface, indicating the formation of Fe_4-N-C active site.[28] As for the high resolution XPS of N 1s and Fe 2p (Fig. 4c,d), it shows the doped-N atoms mainly exist in four different bonding states (Fig. 4c). The peaks at 398.6, 400.1 and 401.4 eV, correspond to pyridinic, pyrrolic and graphitic N, respectively.[29] The fourth peak at 399.6 eV could be attributed to the Fe-N bond within the Fe-$N_{4/2}$-C active site.[30] It has been known all these *n*-type doping of N on carbon can form disordered local structure, and then activate the oxygen reduction reaction.[31] As for the Fe 2p shown in Fig. 4d, it can be divided into three peaks at 706.4 (Fe^0), 710.5 (Fe^{3+}) and 712.4 (Fe^{2+}),[32] further confirming the coexistence of Fe^0 and iron oxides as observed from TEM. The above result is further confirmed by the X-ray diffraction (XRD) analysis as shown in Fig. S8 which shows the formation of Fe^0, Fe_3O_4 and Fe_4N but without Fe_3C (iron carbide).[33]

Conclusions

To sum up, a high performance BP_{ox}-NFe catalyst has been prepared based on cheap carbon black. The optimal catalyst reveals excellent activity for ORR in both alkaline and acidic media. The maximum power densities of alkaline H_2-O_2 and direct methanol fuel cells with the optimal BP_{ox}-NFe as cathode are 107 mW/cm^2 at 50^{o}C and 49.3 mW/cm^2 at 60^{o}C, respectively. The high-performance and low-cost of the optimal BP_{ox}-NFe catalyst make its performance/price ratio superhigh and one of the most promising alternatives to Pt-based catalysts for fuel cell development. Moreover, the following catalytic activity order of different active sites in Fe-N_x/C catalysts was revealed: Fe-$N_{4/2}$-C > Fe_4-N-C > N-C >> Fe_4-C ≈ C.

This work was funded by the National Basic Research Program of China (973 Program, 2012CB932800 and 2014CB932700), National Natural Science Foundation of China (21273220 and 21073180), and "the Recruitment Program of Global youth Experts" of China.

Notes and references

[a] State Key Laboratory of Electroanalytical Chemistry, & Jilin Province Key Laboratory of Low Carbon Chemical Power, Changchun Institute of Applied Chemistry, Chinese Academy of Science, 5625 Renmin Street, Changchun 130022, P.R. China. Tel: 86-431-85262848. E-mail: weilinxu@ciac.ac.cn
[b]College of Chemistry and Molecular Sciences, Hubei Key Lab of Electrochemical Power Sources, Wuhan University, Wuhan 430072, China.

Electronic Supplementary Information (ESI) available: Catalyst preparation, XPS, Electrochemical measurements, Membrane assembly electrode preparation and fuel cell test. See DOI: 10.1039/c000000x/

1. M. K. Debe, *Nature*, 2012, **486**, 43-51.
2. K. Gong, F. Du, Z. Xia, M. Durstock and L. Dai, *Science*, 2009, **323**, 760-764.
3. Y. Li, W. Zhou, H. Wang, L. Xie, Y. Liang, F. Wei, J. Idrobo, S. J. Pennycook and H. Dai, *Nat. Nanotechnol.*, 2012, **7**, 394-400.
4. L. Yang, S. Jiang, Y. Zhao, L. Zhu, S. Chen, X. Wang, Q. Wu, J. Ma, Y. Ma and Z. Hu, *Angew. Chem. Int. Ed.*, 2011, **50**, 7132-7135.
5. Z.-W. Liu, F. Peng, H.-J. Wang, H. Yu, W.-X. Zheng and J. Yang, *Angew. Chem. Int. Ed.*, 2011, **50**, 3257-3261.
6. H. T. Chung, J. H. Won and P. Zelenay, *Nat. Commun.*, 2013, **4**, 1922-1926
7. M. Lefèvre, E. Proietti, F. Jaouen and J.-P. Dodelet, *Science*, 2009, **324**, 71-74.
8. H. W. Liang, W. Wei, Z. Wu, X. Feng and K. Müllen, *J. Am. Chem. Soc.*, 2013, **135**, 16002-16005.
9. J. Liu, X. Sun, P. Song, Y. Zhang, W. Xing and W. Xu, *Adv. Mater.*, 2013, **25**, 6879-6883.
10. D. Deng, L. Yu, X. Chen, G. Wang, L. Jin, X. Pan, J. Deng, G. Sun and X. Bao, *Angew. Chem., Int. Ed.*, 2013, **52**, 371-375.
11. R. Cao, R. Thapa, H. Kim, X. Xu, M. G. Kim, Q. Li, N. Park, M. Liu and J. Cho, *Nat. Commu.*, 2013, doi:10.1038/ncomms3076.
12. J. Tian, A. Morozan, M. T. Sougrati, M. Lefèvre, R. Chenitz, J. P. Dodelet, D. Jones and F. Jaouen, *Angew. Chem.*, 2013, **125**, 7005-7008.
13. E. Proietti, F. Jaouen, M. Lefèvre, N. Larouche, J. Tian, J. Herranz and J.-P. Dodelet, *Nat. Commu.*, 2011, **2**, 416.
14. G. Wu, K. L. More, C. M. Johnston and P. Zelenay, *Science*, 2011, **332**, 443-447.
15. W. Li, J. Wu, D. C. Higgins, J. Y. Choi and Z. Chen, *ACS Catal.*, 2012, **2**, 2761-2768.
16. G. Wu, C. M. Johnston, N. H. Mack, K. Artyushkova, M. Ferrandon, M. Nelson, J. S. Lezama-Pacheco, S. D. Conradson, K. L. More, D. J. Myersd and P. Zelenay, *Journal of Materials Chemistry*, 2011, **21**, 11392-11405.
17. Y. Liang, Y. Li, H. Wang, J. Zhou, J. Wang, T. Regier and H. Dai, *Nat. Mater.*, 2011, **10**, 780-786.
18. G. Hu, F. Nitze, E. Gracia-Espino, J. Ma, H. R. Barzegar, T. Sharifi, X. Jia, A. Shchukarev, L. Lu, C. Ma, G. Yang and T. Wagberg, *Nat. Comm.*, 2014, **5**, 1-8.
19. W. Yang, T. P. Fellinger and M. Antonietti, *J. Am. Chem. Soc.*, 2011, **133**, 206-209.
20. A. Damjanovic and M. A. Genshaw, *Electrochimica Acta*, 1970, **15**, 1281-1283.
21. W. Xia, J. Masa, M. Bron, W. Schuhmann and M. Muhler, *Electrochem. Commun.*, 2011, **13**, 593-596.
22. G. Ma, R. Jia, J. Zhao, Z. Wang, C. Song, S. Jia and Z. Zhu, *J. Phys. Chem. C*, 2011, **115**, 25148-25154.
23. X. Sun, P. Song, Y. Zhang, C. Liu, W. Xu and W. Xing, *Sci. Rep.*, 2013, **3**, 2505-2509.
24. X. Sun, Y. Zhang, P. Song, J. Pan, L. Zhuang, W. Xu and W. Xing, *ACS Catal.*, 2013, **3**, 1726-1729.
25. E. H. Yu, K. Scott and R. W. Reeve, *J. Appl. Electrochem.* , 2006, **36**, 25-32.
26. M. Lefèvre, J. P. Dodelet and P. Bertrand, *J Phys. Chem. B*, 2002, **106**, 8705-8713.
27. G. Kawamura, Y. Tsurumi, H. Muto, M. Sakai, M. Inoue and A. Matsuda, *Mater. Chem. Phys.*, 2011, **130**, 264-269.
28. S. Matar, P. Mohn, G. Demazeau and B. Siberchicot, *J. Phys. France*, 1988, **49**, 1761-1768.
29. S. Yang, X. Feng, X. Wang and K. Müllen, *Angew. Chem. Int. Ed.*, 2011, **50**, 5339-5343.
30. H. Peng, Z. Mo, S. Liao, H. Liang, L. Yang, F. Luo, H. Song, Y. Zhong and B. Zhang, *Sci. Rep.*, 2013, doi:10.1038/srep01765
31. G. Wu, D. Li, C. Dai, D. Wang and N. Li, *Langmuir*, 2008, **24**, 3566-3575.
32. L. Wang, J. Yin, L. Zhao, C. Tian, P. Yu, J. Wang and H. Fu, *Chem. Comm.*, 2013, **49**, 3022-3024.
33. Y. Hu, J. O. Jensen, W. Zhang, L. N. Cleemann, W. Xing, N. J. Bjerrum and Q. Li, *Angew. Chem., Int. Ed.*, 2014, **53**, 3675-3679.

